Supplement to: An example of how data quality hinders progress: translating the latest findings on the regulation of leaf senescence timing in trees into the DP3 model (v1.0)

Michael Meier*[1], Christof Bigler[2], Isabelle Chuine[1]

[1] Centre d'Ecologie Foncitonelle et Evolutive, CNRS, Montpellier, France

[2] Forest Ecology, Department of Environmental Systems Science, ETH Zurich, Zurich, Switzerland

Correspondence to: Michael Meier, (michael.meier@cefe.cnrs.fr)

S1 Data

S1.1 Coordinate transformation

The coordinates of the Swiss sites (Swiss phenology network, 2025) were transformed from the Swiss LV03 North and East projections (x and y [m]) to WGS84 latitude and longitude (φ and λ [°], respectively; Eqs. S1–S6; Sect. 2 in Geodesy, 2016):

$$x' = (x - 200000\,\mathrm{m}) / 1000000 \tag{S1}$$

$$y' = (y - 600000\,\mathrm{m}) / 1000000 \tag{S2}$$

$$\phi' = 2.6779094 + 4.728982\, y' + 0.791484\, y' x' + 0.1306\, y' x'^2 - 0.0436\, y'^3 \tag{S3}$$

$$\lambda' = 16.9023892 + 3.238272\, x' - 0.270978\, y'^2 - 0.002528\, x'^2 - 0.0447\, y'^2 x' - 0.0140\, x'^3 \tag{S4}$$

$$\phi = \phi' / 0.36 \tag{S5}$$

$$\lambda = \lambda' / 0.36 \tag{S6}$$

S1.2 Driver calculations

S1.2.1 Day length

Day length (L_{doy}) for a given day of year (doy [d]) was calculated from φ according to Eqs. 1, 3, and 4 in Brock (1981; Eqs. S7–S9):

$$\gamma_{doy} = 23.45\,°\sin\left(360\,°\left(doy - 81\right)/365\right) \tag{S7}$$

$$W_{doy} = \arccos\left(-\tan\left(\varphi\right) * \tan\left(\gamma_{doy}\right)\right) \tag{S8}$$

$$L_{doy} = 2\frac{W_{doy}}{15\,°\,\mathrm{h}^{-1}} \tag{S9}$$

With γ_{doy} and W_{doy} being the respective declination [°] and hour-angle [°] at sunrise at *doy*.

S1.2.2 Photosynthetic activity

Sink limited daily net photosynthetic activity (A_{net} [mol C d^{-1}]; Collatz et al., 1991) was calculated as the difference between the gross photosynthetic activity (A_{grs} [mol C d^{-1}]) and respiration (R [mol C d^{-1}]; Collatz et al., 1991; Farquhar et al., 1980; Wohlfahrt and Gu, 2015). A_{grs} in turn depended on photon availability (J_E [mol C d^{-1}]), Rubisco activity (J_C [mol C d^{-1}]), and sink capacity (J_S [mol C d^{-1}]), while R was defined as a fraction of the maximum photosynthetic rate (V_{max} [mol C d^{-1}]; Eqs. S10–S13).

$$A_{net} = A_{grs} - R \tag{S10}$$

$$A_{grs} = \max\left(0,\quad L \times \frac{J_P + J_S - \sqrt{\left(J_P + J_S\right)^2 - 4\beta_C J_P J_S}}{2\beta_C}\right) \tag{S11}$$

$$R = b_{C3} V_{max} \qquad \text{(S12}$$

J_P is an intermediate variable, combining J_E and J_C (Eq. S13). β_C is a constant shape parameter, and b_{C3} is a constant fraction for C3 plants (Table S1). J_E and J_C are daily fractions of the available photosynthetically active radiation ($APAR$ [W m^{-2}]) and V_{max}, respectively, while J_S is a constant fraction of V_{max} (Eq. S14–S16).

$$J_P = \frac{J_C + J_E - \sqrt{\left(J_C + J_E\right)^2 - 4\theta_C J_E J_C}}{2\theta_C} \tag{S13}$$

$$J_E = C_1 \times {}^{APAR}\!\big/_{L} \tag{S14}$$

$$J_C = C_2 \times {}^{V_{max}}\!\big/_{24[\mathrm{h}]} \tag{S15}$$

$$J_S = 0.5 \times {}^{V_{max}}\!\big/_{24[\mathrm{h}]} \tag{S16}$$

Here, θ_C is a constant shape parameter (Table S1) and L is the day length [h]. V_{max} depended on *APAR* (Eq. S17), which in turn was calculated as a fraction (*fapar*) of the photosynthetically active radiation (*PAR* [W m^{-2}]; Eq. S18). While *fapar* depended on the leaf area index (*LAI*; Eq. S19), *PAR* was derived from the surface shortwave down welling radiation (R_s [W m^{-2}]; Eq. S20).

$$V_{max}=1/b_{C3}\,C_1/C_2\,[(2\theta-1)s-\sigma(2\theta s-C_2)]\,APAR \quad \text{(S17)}$$

$$APAR=\alpha_a c_q\, fapar\, PAR\,(3600\times24)[\mathrm{s}] \quad \text{(S18)}$$

$$fapar=1\,e^{-0.5\,LAI} \quad \text{(S19)}$$

$$PAR=0.5\,R_s \quad \text{(S20)}$$

Here, θ is a constant shape parameter, while α_a and c_q are a constant ratio and a constant conversion factor for the respective assimilation and conversion of solar radiation (Table S1). V_{max} depends on s and σ (Eqs. S21 and S22) as well as on C_1 and C_2 (Eqs. S23 and S24).

$$\sigma=\sqrt{1-C_2-s/C_2-\theta s} \quad \text{(S21)}$$

$$s=b_{C3}\,24[\mathrm{h}]/L \quad \text{(S22)}$$

$$C_1=\phi_C\,\alpha_{C3}\,f(T)\times p_{i,CO2}-\Gamma_*/p_{i,CO2}+2\Gamma^* \quad \text{(S23)}$$

$$C_2=\frac{(p_{i,CO2}-\Gamma_*)}{p_{i,CO2}+K_C(1+p_{a,O2}/K_O)} \quad \text{(S24)}$$

α_{C3} describes the quantum efficiency of C3 plants, and $p_{a,O2}$ is the ambient partial O_2 pressure (Table S1). $p_{i,CO2}$ is the internal partial CO_2 pressure (Eq. S25), Γ_* is the CO_2 condensation point (Eq. S26), K_C and K_O are the kinetic coefficients for CO_2 and O_2, respectively (Eqs. S27 and S28), and *f(T)* is a function of the mean temperature (Eq. S29).

$$p_{i,CO2}=\lambda_{C3}[CO_2]_A\,10^{-16}\,p_0 \quad \text{(S25)}$$

$$\Gamma_* = p_{a,O2} \big/ 2\tau q_{\tau 10}^{(T-25K)/10} \tag{S26}$$

$$K_C = k_C q_{C10}^{(T-25\mathrm{K})/10} \tag{S27}$$

$$K_O = k_O q_{O10}^{(T-25\mathrm{K})/10} \tag{S28}$$

$$f(x) = \min\left(1, \quad \max\left(0, \quad 1 \big/ 1+e^{k_1(k_2-T)} \times \left(1-0.01\, e^{k_3(T-x_3)}\right)\right)\right) \tag{S29}$$

Here, λ_{C3} is the optimal ratio of internal to ambient CO_2 pressure of C3 plants. τ, k_C, and k_O are the specificity ratio CO_2:O_2 and the Michaelis constants for CO_2 and O_2, respectively, while $q_{\tau 10}$, q_{C10}, and q_{O10} are the corresponding rates of change due to a 10 K change in mean temperature (T [°C]). k_1, k_2, and k_3 are derived from the cardinal temperatures x_1, x_2, x_3, and x_4 (Eqs. S30–S32, Table S1).

$$k_1 = 2\log(1/0.99-1) \big/ x_1 - x_2 \tag{S30}$$

$$k_2 = (x_1 + x_2)/2 \tag{S31}$$

$$k_3 = \log\left(0.99/0.01 \big/ x_4 - x_3\right) \tag{S32}$$

Table S1. Constants.

Constant	Value	Description	Source
β_C	0.95	Fraction; Co-limitation (shape) parameter for J_P and J_S	Co97, Eq. (A9)
b_{C3}	0.015	Fraction; Leaf respiration per maximum Rubisco capacity for C3 plants	HP96, Table 2
θ_C	0.98	Fraction; Co-limitation (shape) parameter for J_C and J_E	Co97, Eq. (A8)
θ	0.7	Fraction; Alternative co-limitation (shape) parameter for J_C and J_E	Table 2 in HP96
α_a	0.5	Ratio; Assimilated PAR from ecosystem to leaf level	Table 4 in Si00
c_q	4.6×10^{-6}	[E J^{-1}], [mol J^{-1}]; Conversion factor for solar radiation at 550 nm	
α_{C3}	0.08	Intrinsic quantum efficiency of CO_2 uptake in C3 plants	Ha96; Si00
p_0	1.013×10^5	[Pa]; Standard pressure	-
$P_{a,O2}$	$0.209 \times p_0$	[Pa]; Ambient O_2 pressure	Table A1 in Co97; Table 2 in HP96
λ_{C3}	0.8	Fraction	Ge04
τ	2600	Ratio; CO_2:O_2 specificity ratio	Table A1 in Ca91
k_O	3×10^4	[Pa]; Michaelis constant for O_2	Table A1 in Co97; Table 2 in HP96
k_C	30	[Pa]; Michaelis constant for CO_2	
$q_{\tau 10}$	0.57	Fraction; Temperature-sensitivity of τ regarding a change of 10 K	Table A1 in Ca91
q_{O10}	1.2	Fraction; Temperature-sensitivity of k_O regarding a change of 10 K	Table A1 in Co97; Table 2 in HP96
q_{C10}	1.2	Fraction; Temperature-sensitivity of k_C regarding a change of 10 K	
x_1	1	[°C]; Cardinal temperatures	Eqs. S10–S15 in Za20
x_2	18		
x_3	25		
x_4	45		

Note: These constants were taken from following sources: Co91: (Collatz et al., 1991); Ge04: (Gerten et al., 2004); Ha96: (Haxeltine et al., 1996); HP96: (Haxeltine and Prentice, 1996); Si00: (Sitch et al., 2000); Za20: (Zani et al., 2020).

S1.2.3 Keetch and Byram drought index

The Keetch and Byram drought index for day *i* (Q_i; Eq. S33) was calculated from daily precipitation (P_i) and daily maximum temperature (Tx_i; Keetch and Byram, 1968), which were converted from millimeters [mm] to inches [in] and from degree Celsius [°C] to degree Fahrenheit [°F], respectively (P'_i and Tx'_i; Eqs. S34 and S35; Foster et al., 1981, Table 2; Shaw, 1931; Woods, 1931):

$$Q_i = \min\left(800, \quad \max\left(0, \quad Q_{Base,i} + \Delta Q_i\right)\right) \tag{S33}$$

$$P'_i = P_i \Big/ 25.4\left[\text{mm in}^{-1}\right] \tag{S34}$$

$$Tx'_i = 9/5\left[°\text{F } °\text{C}^{-1}\right] \times Tx_i + 32\left[°\text{F}\right] \tag{S35}$$

The base index ($Q_{base,i}$) was derived from Q of the previous day (i.e., Q_{i-1}) and the net precipitation of the given day ($P_{net,i}$ [in]; Eq. S36), while the daily drought factor (ΔQ_i) was calculated from the base index ($Q_{base,i}$), Tx'_i, and mean annual rainfall (R_i, [in]; Eqs. S37–S38):

$$Q_{Base,i} = \max(0, \quad Q_{i-1} - 100\, P_{net,i}) \tag{S36}$$

$$\Delta Q_i = (800 - Q_{Base,i}) \times \frac{0.968\, e^{0.0486\, Tx'_i} - 0.83}{1 + 10.88\, e^{-0.0441\, R_i}} \times 0.001 \tag{S37}$$

$$R_i = \frac{1}{366} \sum_{j=i-355}^{i} P'_j \tag{S38}$$

Here, $Q_{Base,1}$ (i.e., of January 1st, 1950) was set to the average Q_{Base} during the Decembers and Januaries of 1955–1959, $R_1, R_2, \ldots, R_{355} = R_{366}$, and $P'_i = 0$ if the precipitation fell as snow (i.e., if the mean temperature $T_i \leq 0$ °C). P_{net} depends on P' of the given and two previous days in comparison to a threshold precipitation of 0.2 in (Y_P; Eq. S39).

$$P_{net,i} = \begin{cases} \max(0, \quad P'_i - Y_P) & , \quad if \quad P'_{i-1} = 0 \\ P'_i & , \quad if \quad P'_{i-1} \geq Y_P \\ \max\left(0, \quad \sum_{k=0}^{1} P'_{i-k} - Y_P\right) & , \quad if \quad P'_{i-1} < Y_P \quad \wedge \quad \sum_{k=1}^{2} P'_{i-k} \geq Y_P \\ \max\left(0, \quad \sum_{k=0}^{2} P'_{i-k} - Y_P\right) & , \quad if \quad P'_{i-1} < Y_P \quad \wedge \quad \sum_{k=1}^{2} P'_{i-k} < Y_P \end{cases} \tag{S39}$$

The KBDI was initiated per site, i.e., setting Q_i to zero after the first period of either abundant precipitation or snow melt during 1950–1954 (Keetch and Byram, 1968). A period of abundant precipitation was defined as seven consecutive days during which the precipitation sum was six inches (i.e., 152.4 mm; see Eq. S34) or more. A period of snow melt was defined as four consecutive days during which the snow melt followed on at least seven days with snow fall. For this, we defined day *i* as a day with snow melt when $T_i > 0$ °C and as a day with snow fall when $P_i > 0$ mm and $T_i \leq 0$ °C.

S2 Methods

S2.1 Controls of the simulated annealing algorithm

The choice of the controls for the optimization algorithm influences the accuracy of the calibrated model (Meier and Bigler, 2023) through the exploration–exploitation trade-off (Candelieri, 2021; Maes et al., 2013). Thus, we set the controls ‘maximum iterations’, ‘maximum calls’, and ‘temperature’ of the generalized simulated annealing algorithm (Xiang et al., 1997, 2017) such a way that the calibrated model resulted in most accurate simulations for the validation sample. To identify these optimal controls for each model and calibration sample, we calibrated each model four times (i.e., twice with each sample draw) with all 27 combinations of 4000, 5000, and 6000 maximum iterations, 10^6, 10^7, and

10^8 maximum calls, as well as temperatures of 5200, 5230, and 5300. Thus, we used the combination of controls that resulted in the lowest average Akaike information criterion for small samples (i.e., n < 40k; AICc; Eq. S40; based on the validation sample; Akaike, 1974; Burnham and Anderson, 2004) to compute the additional six calibration runs (i.e., three per calibration sample; Table S2).

$$AICc = AIC + \frac{2k(k+1)}{n-k-1} \tag{S40}$$

$$AIC = -2 \times \log(L) + 2k \tag{S41}$$

$$\sigma_e = \sqrt{\frac{1}{n}\sum_{i=1}^{n}(x_{s,i} - x_{o,i})^2} \tag{S42}$$

Here, n is the number of observed and simulated doy pairs (x_o and x_s, respectively) and k is the number of free model parameters. L is the likelihood for the normally distributed model errors (i.e., $x_s - x_o$; Fisher and Russell, 1997) with $N(0, \sigma_e)$. In case $S_{Senescence}$ did not reach the thresholds Y_{LS50} and Y_{LS100} until December 31st, corresponding x_s were considered missing and thus set to doy 367 before their accuracy was evaluated.

Table S2. Optimal controls of the generalized simulated annealing algorithm.

Model	Sample	Maximum iterations	Maximum calls	Temperature
CDD	LS_{50}	4000	10^8	5300
DM2	LS_{50}	6000	10^6	5300
PIA	LS_{50}	5000	10^7	5200
DP3	LS_{50}	4000	10^8	5300
	LS_{50}-LS_{100}	5000	10^7	5200

Note: Only the control settings for the evaluated models (LS_{50} sample) and for the model that was selected through the iterations of model development (LS_{50}-LS_{100} sample) are shown. Those for the models that were rejected during model development are omitted.

S2.2 Model calibration, selection, and evaluation

All models were calibrated by minimizing the root mean squared error (RMSE; Eq. S43).

$$RMSE = \sqrt{\frac{1}{n}\sum_{i=1}^{n}(x_{s,i} - x_{o,i})^2} \tag{S43}$$

Thus, for each model, we selected and further evaluated the calibration run that resulted in highest modified Kling-Gupta efficiency (KGE’; Eq. S44; Gupta et al., 2009; Kling et al., 2012) for the validation sample.

$$KGE' = 1 - \sqrt{(\rho - 1)^2 + (\beta - 1)^2 - (\gamma - 1)^2} \tag{S44}$$

$$\beta = {}^{\mu_s}\!\big/_{\mu_o} \tag{S45}$$

$$\gamma = \frac{\sigma_s / \mu_s}{\sigma_o / \mu_o} \tag{S46}$$

Here, β is the bias ratio, γ is the variability ratio, and ρ is the Pearson correlation between x_o and x_s. μ_o and μ_s, are the respective observed and simulated mean doy, and σ_o and σ_s are the corresponding standard deviations. For the perfect model (i.e., $x_o = x_s$ for all i), $\rho = 1$, $\beta = 1$, and $\gamma = 1$, and thus $KGE' = 1$, whereas $1 > KGE' > -\infty$ for imperfect models.

S2.3 Linear mixed-effects model and analysis of variance

We fitted the following linear mixed-effects model (LMM; Pinheiro and Bates, 2000; Wood, 2011, 2017) to the analyze the effects on the model error:

$$\mathbf{y} = \mathbf{X}\boldsymbol{\beta} + \mathbf{Z}\mathbf{b} + \boldsymbol{\epsilon} \tag{S47}$$

with $\mathbf{y}$ being the n-dimensional vector of the response variable ‘model error’ (ME). $\mathbf{X}$ is the $n \times p$ matrix of the intercept (i.e., 1) and the $p - 1$ explanatory variables. $\boldsymbol{\beta}$ is the corresponding p-dimensional vector of the fixed effects ‘country’ and ‘model’ as well as the annual and site-specific deviations in mean annual temperature, mean annual KBDI, accumulated A_{net} between LU and summer solstice, latitude, and elevation (CTR, MOD, δMAT, δMAQ, δA_{net}, δLAT and δELV, respectively) from the overall calibration sample means per variable. $\mathbf{Z}$ is the $n \times q$ matrix of the random-effects, assigning the n observations to the q groups of the grouping variable ‘site’ (STE). $\mathbf{b}$ is the corresponding q-dimensional vector of the random intercepts with $\mathbf{b} \sim N(0, \sigma^2_{\mathbf{b}} \mathbf{I}_q)$, and $\boldsymbol{\epsilon}$ is the n-dimensional vector of the errors with $\boldsymbol{\epsilon} \sim N(0, \sigma^2 \mathbf{I}_n)$ (Baayen et al., 2008; Chpt. 2.1 in Pinheiro and Bates, 2000; Chpt. 6.2 in Wood, 2017).

We fitted this LMM with the function bam in the R package mgcv (Wood, 2017), using the following formula (Eq. S48):

```
ME ~ MOD * (δMAT + δMAQ + δA_net + δLAT + δELV) + CTR + s(STE, bs = 're')
```
(S48)

This LMM combined effects due to climatic deviations from the calibration sample (red), spatial deviations from the calibration sample (green), and data structure (blue). The LMM was the basis for the type-III ANOVA (Yates, 1934), which we derived with the functions aov and drop1 in the R package stats (Eq. S49; R Core Team, 2022):

```
drop1(aov(LMM), scope = ~., test = "F")
```
(S49)

Thus, we calculated the amount of variation attributed to differences among each explanatory variable, i.e., the relative impact of given variable on the variance in the model error explained by the LMM, by dividing the variable-specific sum of squares by the total sum of squares over all variables.

S3 Results

S3.1 Formulation of the leaf development process

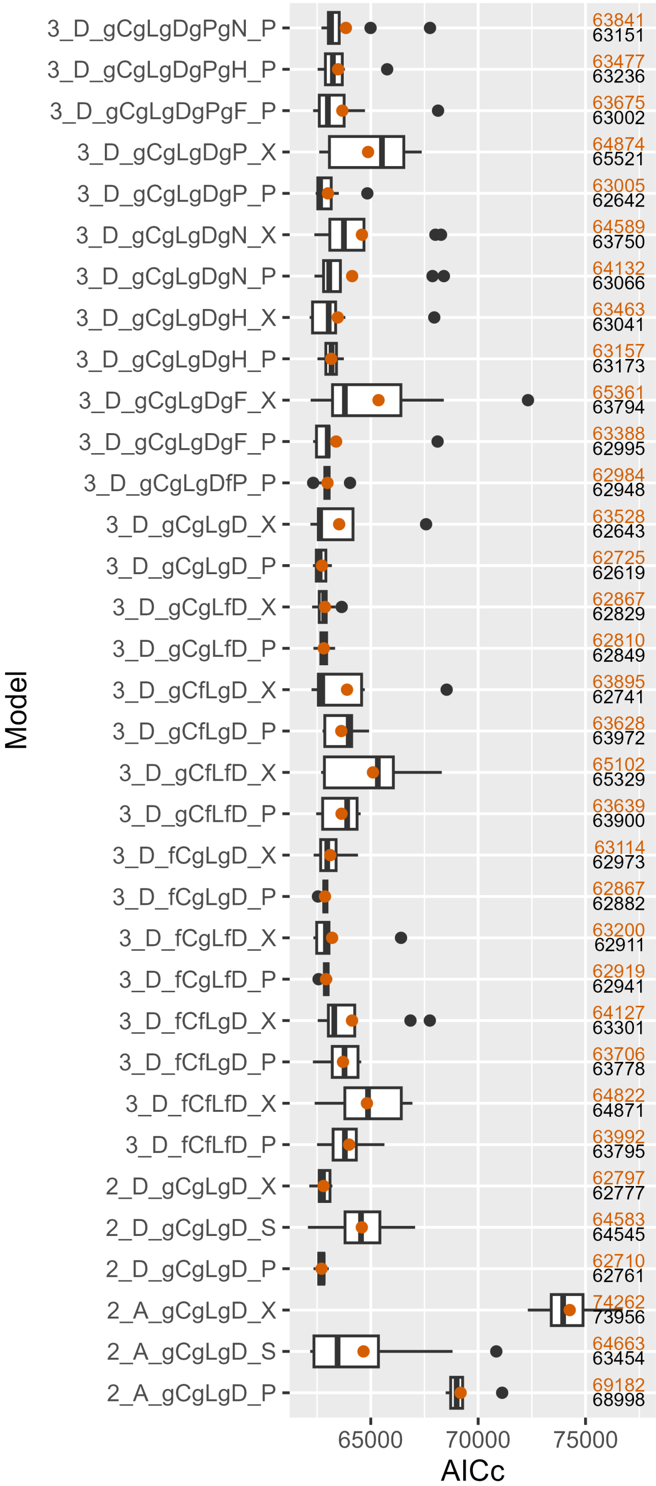

Figure S1. Accuracy of models to test the formulations of the leaf development process. The accuracy was assessed with the Akaike information criterion for small samples (AICc; Eq. S40). The boxes indicate the inner quartile range and the median (middle line). The most extreme values are indicated with dots if outside ±1.5 times the inner quartile range from the 1st and 3rd quartile, and with whiskers otherwise. Orange dots show the mean, which is further indicated in orange to the right of each box, together with the median indicated in black. The models were labeled as $x_P\_x_A\_x_S\_x_X$, with x_P being the number of leaf development phases (i.e., 2 or 3), x_A being the driver of the aging rate (i.e., A or D for photosynthesis or days, respectively), x_S being the stress rate that is the summed response [i.e., g or h for *g(x)* or *h(x)*] to the drivers cold, shortening, dry, heat, and frost days, heavy rainfall, and nutrient depletion (i.e., C, L, D, H, F, P, and N, respectively), and x_X indicating the formulation of the senescence rate (i.e., S, P, or X when formulated as a sum, product, or exponential function of aging and stress, respectively). All models were calibrated with the LS_{50}-LS_{100} sample (Sect. 2.4).

Table S3. The cause of senescence induction and corresponding prevailing conditions

Calibration	Cause	Number	Variable	Minimum	Maximum	Median	Mean
LS_{50}	Stress	6677	MAT [°C]	3.78	15.36	8.80	8.72
			MAQ	2.78	106.42	8.48	10.27
			LAT [°]	45.86	57.98	47.78	48.92
			ELV [m a.s.l.]	0	1440	450	473.22
	Aging	162	MAT [°C]	5.76	14.40	9.99	10.02
			MAQ	4.81	59.89	10.92	13.74
			LAT [°]	45.87	54.52	48.98	49.38
			ELV [m a.s.l.]	5	920	320	314.51
	Both	48	MAT [°C]	5.24	12.08	9.98	9.80
			MAQ	4.11	51.49	10.95	13.80
			LAT [°]	45.86	54.75	48.73	49.10
			ELV [m a.s.l.]	13	920	400	372.31

Note: In the DP3 model, senescence is induced with the transition from the leaf development phase ‘mature leaf’ to the leaf development phase ‘old leaf’. This transition is caused by either or both the accumulated aging and stress rate reaching their corresponding thresholds (here indicated with the ‘Cause’ being ‘Aging’, ‘Stress’, or ‘Both’). We summed the number of the given causes as well as summarized the prevailing conditions that corresponded to these causes according to the variables mean annual temperature (MAT), mean annual KBDI (MAQ), latitude (LAT), and elevation (ELV). The model was calibrated with the LS_{50} sample (Sect. 2.4).

Table S4. The relative importance of the stressors for stress caused senescence induction

Calibration	Stress	Average	Dimension	Minimum	Maximum	Median	Mean
LS_{50}	Cold stress	0.23	MAT [°C]	0.09	0.40	0.26	0.26
			MAQ	0.04	0.61	0.22	0.28
			LAT [°]	0.12	0.26	0.22	0.21
			ELV [m a.s.l.]	0.05	0.28	0.17	0.17
	Photoperiod stress	0.77	MAT [°C]	0.60	0.91	0.74	0.74
			MAQ	0.39	0.96	0.78	0.72
			LAT [°]	0.74	0.88	0.78	0.79
			ELV [m a.s.l.]	0.72	0.95	0.83	0.82
	Dry stress	0.000	MAT [°C]	0.000	0.000	0.000	0.000
			MAQ	0.000	0.000	0.000	0.000
			LAT [°]	0.000	0.000	0.000	0.000
			ELV [m a.s.l.]	0.000	0.000	0.000	0.000

Note: We compared the relative amount of accumulated cold, photoperiod, and dry stress at the day of stress caused senescence induction. To do so, we calculated the overall average for each stressor as well as the average for each of five bins of equal width across the dimensions mean annual temperature (MAT), mean annual KBDI (MAQ), latitude (LAT), and elevation (ELV; Fig. 5). The latter were summarized into the minimum, maximum, median, and mean average across these bins. The model was calibrated with the LS_{50} sample (Sect. 2.4).

S3.2 Model error

Table S5. Linear mixed-effects model (LMM) coefficients of fixed effects explaining the model error

Coefficient	**Value**	**SE**	***t* statistic**	***p*-value**	**$\underline{BF}_{01}$**	**Lower 0.5%**	**Upper 99.5%**
Intercept	8.1084	4.8078	1.6865	0.0917	0.6707	-4.2762	20.4929
CDD [d]	-1.8477	0.2294	-8.0554	**0.0000**	**0.0000**	-2.4386	-1.2569
DM2 [d]	-0.7681	0.2294	-3.3485	**0.0008**	0.0203	-1.3589	-0.1772
PIA [d]	-0.7898	0.2432	-3.2475	**0.0012**	0.0275	-1.4162	-0.1633
DP3 [d]	0.0705	0.2294	0.3073	0.7586	1.0000	-0.5204	0.6613
δMAT [d °C^{-1}]	-1.9833	0.0979	-20.2533	**0.0000**	**0.0000**	-2.2356	-1.7311
δMAQ [d]	0.0704	0.0125	5.6407	**0.0000**	**0.0000**	0.0382	0.1025
δA_{net} [d mol C^{-1} m^{-2}]	0.4129	0.0119	34.7527	**0.0000**	**0.0000**	0.3823	0.4435
δLAT [d °$^{-1}$]	-18.2749	0.6851	-26.6755	**0.0000**	**0.0000**	-20.0396	-16.5102
δELV [d m^{-1}]	-0.1013	0.0050	-20.2933	**0.0000**	**0.0000**	-0.1141	-0.0884
SUI [d]	-22.0962	5.9671	-3.7030	**0.0002**	*0.0064*	-37.4669	-6.7255
GER [d]	11.2441	6.7837	1.6575	0.0974	0.6919	-6.2303	28.7184
GBR [d]	13.8831	8.1882	1.6955	0.0900	0.6641	-7.2089	34.9751
CDD × δMAT [d °C^{-1}]	-0.1713	0.1706	-1.0038	0.3155	1.0000	-0.6108	0.2682
DM2 × δMAT [d °C^{-1}]	-0.2027	0.1706	-1.1881	0.2348	0.9671	-0.6423	0.2368
PIA × δMAT [d °C^{-1}]	0.0700	0.1707	0.4098	0.6819	1.0000	-0.3698	0.5097
DP3 × δMAT [d °C^{-1}]	-0.0687	0.1706	-0.4026	0.6873	1.0000	-0.5082	0.3708
CDD × δMAQ [d]	-0.0325	0.0245	-1.3280	0.1842	0.9066	-0.0957	0.0306
DM2 × δMAQ [d]	-0.0291	0.0245	-1.1853	0.2359	0.9681	-0.0922	0.0341
PIA × δMAQ [d]	-0.0261	0.0251	-1.0385	0.2990	0.9985	-0.0907	0.0386
DP3 × δMAQ [d]	0.0065	0.0245	0.2644	0.7915	1.0000	-0.0567	0.0696
CDD × δA_{net} [d mol C^{-1} m^{-2}]	0.0196	0.0213	0.9206	0.3573	1.0000	-0.0353	0.0746
DM2 × δA_{net} [d mol C^{-1} m^{-2}]	0.0117	0.0213	0.5482	0.5836	1.0000	-0.0433	0.0666
PIA × δA_{net} [d mol C^{-1} m^{-2}]	0.0489	0.0213	2.2941	0.0218	0.2723	-0.0060	0.1038
DP3 × δA_{net} [d mol C^{-1} m^{-2}]	-0.0008	0.0213	-0.0368	0.9707	1.0000	-0.0557	0.0542
CDD × δLAT [d °$^{-1}$]	-0.0987	0.1244	-0.7930	0.4278	1.0000	-0.4191	0.2218
DM2 × δLAT [d °$^{-1}$]	-0.1079	0.1244	-0.8669	0.3860	1.0000	-0.4283	0.2126
PIA × δLAT [d °$^{-1}$]	-0.0751	0.1246	-0.6031	0.5465	1.0000	-0.3961	0.2458
DP3 × δLAT [d °$^{-1}$]	-0.0242	0.1244	-0.1943	0.8460	1.0000	-0.3446	0.2963
CDD × δELV [d m^{-1}]	-0.0013	0.0011	-1.1367	0.2557	0.9822	-0.0042	0.0016
DM2 × δELV [d m^{-1}]	-0.0012	0.0011	-1.0723	0.2836	0.9949	-0.0042	0.0017
PIA × δELV [d m^{-1}]	-0.0015	0.0011	-1.2759	0.2020	0.9321	-0.0044	0.0015
DP3 × δELV [d m^{-1}]	-0.0001	0.0011	-0.0776	0.9382	1.0000	-0.0030	0.0029

Note: The LMM was fitted to the response variable 'model error' [i.e., $x_{s,i} - x_{o,i}$, the difference in days calculated as the simulated minus the observed date for each stage and site year (i)] in the validation sample (Sect. 2.6 and S2.3), based on 54 834 observations, and resulted in an adjusted R^2 of 0.48 and a proportion of the deviance explained of 0.48. The random intercepts were grouped by site with σ_b = 31.38 d (99% confidence interval 27.70 ≤ σ_b ≤ 35.55 d). SE is the standard error, while 'Lower 0.05%' and 'Upper 99.5%' indicate the lower and upper boundaries of the 99% confidence interval. Bold p-values are indicate significant fixed effects at a = 0.01 (i.e., $p \leq 0.005$ for a two-sided hypothesis test), bold and italic minimum Bayes factors ($\underline{BF}_{01}$) indicate decisive and very strong fixed effects (i.e., $\underline{BF}_{01} \leq 1/1000$ and $\underline{BF}_{01} \leq 1/100$, respectively). The intercept represents the base line, i.e., the model error according to the Null model for Austria. CDD, DM2, PIA, and DP3 are the factorized models, while SUI, GER, and GBR are the factorized countries Switzerland, Germany, and United Kingdom, respectively. The random intercepts were grouped by 'site'. All models ware calibrated and validated with the LS_{50} sample (Sect. 2.4).

Table S6. Interacting effects according to the LMM

Variable	Model	Country	Estimate	SE	0.5 %	99.5 %	Equation
Country [d]	Null	AUT	8.11	4.81	-4.28	20.49	β_0
		SUI	-13.99	4.57	-25.76	-2.21	β_0 + SUI
		GER	19.35	4.11	8.76	29.95	β_0 + GER
		GBR	21.99	5.43	8.01	35.98	β_0 + GBR
	CDD	AUT	6.26	4.84	-6.20	18.72	β_0 + CDD
		SUI	-15.84	4.60	-27.69	-3.98	β_0 + CDD + SUI
		GER	17.50	4.10	6.95	28.06	β_0 + CDD + GER
		GBR	20.14	5.40	6.25	34.04	β_0 + CDD + GBR
	DM2	AUT	7.34	4.84	-5.12	19.80	β_0 + DM2
		SUI	-14.76	4.60	-26.61	-2.90	β_0 + DM2 + SUI
		GER	18.58	4.10	8.03	29.14	β_0 + DM2 + GER
		GBR	21.22	5.40	7.32	35.12	β_0 + DM2 + GBR
	PIA	AUT	7.32	4.78	-5.01	19.64	β_0 + PIA
		SUI	-14.78	4.54	-26.47	-3.08	β_0 + PIA + SUI
		GER	18.56	4.15	7.88	29.24	β_0 + PIA + GER
		GBR	21.20	5.49	7.07	35.33	β_0 + PIA + GBR
	DP3	AUT	8.18	4.84	-4.28	20.64	β_0 + DP3
		SUI	-13.92	4.60	-25.77	-2.07	β_0 + DP3 + SUI
		GER	19.42	4.10	8.87	29.98	β_0 + DP3 + GER
		GBR	22.06	5.40	8.16	35.96	β_0 + DP3 + GBR
δELV [d 100 m^{-1}]	Null	NA	-10.13	0.50	-11.41	-8.84	100 δELV
	CDD		-10.26	0.51	-11.56	-8.95	100 (δELV + CDD × δELV)
	DM2		-10.25	0.51	-11.56	-8.95	100 (δELV + DM2 × δELV)
	PIA		-10.27	0.51	-11.58	-8.97	100 (δELV + PIA × δELV)
	DP3		-10.14	0.51	-11.44	-8.83	100 (δELV + DP3 × δELV)
δLAT [d $°^{-1}$]	Null		-18.27	0.69	-20.04	-16.51	δLAT
	CDD		-18.37	0.69	-20.15	-16.59	δLAT + CDD × δLAT
	DM2		-18.38	0.69	-20.16	-16.60	δLAT + DM2 × δLAT
	PIA		-18.35	0.69	-20.13	-16.57	δLAT + PIA × δLAT
	DP3		-18.30	0.69	-20.08	-16.52	δLAT + DP3 × δLAT
δMAQ [d 100^{-1}]	Null		7.04	1.25	3.82	10.25	100 δMAQ
	CDD		3.78	2.25	-2.02	9.59	100 (δMAQ + CDD × δMAQ)
	DM2		4.13	2.25	-1.67	9.94	100 (δMAQ + DM2 × δMAQ)
	PIA		4.43	2.32	-1.56	10.42	100 (δMAQ + PIA × δMAQ)
	DP3		7.68	2.25	1.88	13.49	100 (δMAQ + DP3 × δMAQ)
δMAT [d 10°C^{-1}]	Null		-19.83	0.98	-22.36	-17.31	10 δMAT
	CDD		-21.55	1.64	-25.78	-17.31	10 (δMAT + CDD × δMAT)
	DM2		-21.86	1.64	-26.09	-17.63	10 (δMAT + DM2 × δMAT)
	PIA		-19.13	1.64	-23.37	-14.90	10 (δMAT + PIA × δMAT)
	DP3		-20.52	1.64	-24.75	-16.29	10 (δMAT + DP3 × δMAT)
δA_{net} [d 10 mol C^{-1} m^{-2}]	Null		4.13	0.12	3.82	4.44	10 δA_{net}
	CDD		4.33	0.20	3.80	4.85	10 (δA_{net} + CDD × δA_{net})
	DM2		4.25	0.20	3.72	4.77	10 (δA_{net} + DM2 × δA_{net})
	PIA		4.62	0.20	4.09	5.14	10 (δA_{net} + PIA × δA_{net})
	DP3		4.12	0.20	3.60	4.65	10 (δA_{net} + DP3 × δA_{net})

Note: The interacting effects of the LMM (Table S5) were calculated with the Delta method (Chpt. 5.1.4 in Fox and Weisberg, 2019; Chpt. 9.9 in Wasserman, 2004) according to the displayed equation, together with their standard error (SE) and 99% confidence interval (i.e., the 0.5% lower bound and 99.5% upper bound). AUT, SUI, GER, and GBR refer to the countries Austria, Switzerland, Germany, and United Kingdom, respectively.

Table S7. Impact on the variance in the model error explained by the LMM

Explanatory variable	**Impact**	**Accumulated**	***p*-value**	$\underline{\mathbf{BF}}_{01}$
Site	0.9191	0.9191	**0.0000**	**0.0000**
δA_{net}	0.0445	0.9636	**0.0000**	**0.0000**
δMAT	0.0150	0.9786	**0.0000**	**0.0000**
δLAT	0.0128	0.9914	**0.0000**	**0.0000**
δELV	0.0056	0.9970	**0.0000**	**0.0000**
Model	0.0019	0.9989	**0.0000**	**0.0000**
δMAQ	0.0007	0.9996	**0.0000**	**0.0001**
Model × δA_{net}	0.0002	0.9998	0.1281	0.7881
Model × δMAT	0.0001	0.9999	0.6440	1.0000
Model × δMAQ	0.0001	1.0000	0.5954	1.0000
Model × δELV	0.0001	1.0001	0.6151	1.0000
Country	0.0000	1.0001	**0.0000**	**0.0000**
Model × δLAT	0.0000	1.0001	0.8702	1.0000

Note: The type-III analysis of variance (ANOVA; Sect. 2.6 and S2.3) was based on the LMM (Table S5) and thus on 54 834 observations. For each explanatory variable (i.e., fixed and random effects), the impact on the variance in the model error as explained by the LMM is given, together with the accumulated impact when ordered by impact. Bold *p*-values are significant at $\alpha = 0.01$ (i.e., $p \leq 0.01$ for a one-sided hypothesis test) and bold minimum Bayes factors ($\underline{\mathrm{BF}}_{01}$) are decisive (i.e., $\underline{BF}_{01} \leq 1/1000$).

References

Akaike, H.: A new look at the statistical model identification, IEEE Trans. Autom. Control, 19, 716–723, 1974.

Baayen, R. H., Davidson, D. J., and Bates, D. M.: Mixed-effects modeling with crossed random effects for subjects and items, J. Mem. Lang., 59, 390–412, https://doi.org/10.1016/j.jml.2007.12.005, 2008.

Brock, T. D.: Calculating solar radiation for ecological studies, Ecol. Model., 14, 1–19, https://doi.org/10.1016/0304-3800(81)90011-9, 1981.

Burnham, K. P. and Anderson, D. R.: Multimodel Inference: Understanding AIC and BIC in Model Selection, Sociol. Methods Res., 33, 261–304, https://doi.org/10.1177/0049124104268644, 2004.

Candelieri, A.: A gentle introduction to Bayesian Optimization, 2021 Winter Simulation Conference (WSC), Phoenix, AZ, and virtual, 1–16, https://doi.org/10.1109/WSC52266.2021.9715413, 2021.

Collatz, G. J., Ball, J. T., Grivet, C., and Berry, J. A.: Physiological and environmental-regulation of stomatal conductance, photosynthesis and transpiration - A model that includes laminar boundary-layer, Agric. For. Meteorol., 54, 107–136, https://doi.org/10.1016/0168-1923(91)90002-8, 1991.

Farquhar, G. D., von Caemmerer, S., and Berry, J. A.: A biochemical model of photosynthetic CO2 assimilation in leaves of C3 species, Planta, 149, 78–90, https://doi.org/10.1007/bf00386231, 1980.

Fisher, R. A. and Russell, E. J.: On the mathematical foundations of theoretical statistics, Philos. Trans. R. Soc. Lond. Ser. Contain. Pap. Math. Phys. Character, 222, 309–368, https://doi.org/10.1098/rsta.1922.0009, 1997.

Foster, G. R., McCool, D. K., Renard, K. G., and Moldenhauer, W. C.: Conversion of the universal soil loss equation to SI metric units, J. Soil Water Conserv., 36, 355–359, 1981.

Fox, J. and Weisberg, S.: An R Companion to Applied Regression, Third., SAGE, Los Angeles, 2019.

Geodesy: Approximate formulas for the transformation between Swiss projection coordinates and WGS84, 2016.

Gerten, D., Schaphoff, S., Haberlandt, U., Lucht, W., and Sitch, S.: Terrestrial vegetation and water balance - hydrological evaluation of a dynamic global vegetation model, J. Hydrol., 286, 249–270, https://doi.org/10.1016/j.jhydrol.2003.09.029, 2004.

Gupta, H. V., Kling, H., Yilmaz, K. K., and Martinez, G. F.: Decomposition of the mean squared error and NSE performance criteria: Implications for improving hydrological modelling, J. Hydrol., 377, 80–91, https://doi.org/10.1016/j.jhydrol.2009.08.003, 2009.

Haxeltine, A. and Prentice, I. C.: BIOME3: An equilibrium terrestrial biosphere model based on ecophysiological constraints, resource availability, and competition among plant functional types, Glob. Biogeochem. Cycles, 10, 693–709, https://doi.org/10.1029/96gb02344, 1996.

Haxeltine, A., Prentice, I. C., and Creswell, D. I.: A coupled carbon and water flux model to predict vegetation structure, J. Veg. Sci., 7, 651–666, https://doi.org/10.2307/3236377, 1996.

Keetch, J. J. and Byram, G. M.: A Drought Index for Forest Fire Control, Department of Agriculture, Forest Service, Southeastern Forest Experiment Station, Asheville, NC: U.S., 1968.

Kling, H., Fuchs, M., and Paulin, M.: Runoff conditions in the upper Danube basin under an ensemble of climate change scenarios, J. Hydrol., 424–425, 264–277, https://doi.org/10.1016/j.jhydrol.2012.01.011, 2012.

Maes, F., Wehenkel, L., and Ernst, D.: Meta-learning of exploration/exploitation strategies: The Multi-armed bandit case, Agents and Artificial Intelligence, 100–115, 2013.

Meier, M. and Bigler, C.: Process-oriented models of autumn leaf phenology: ways to sound calibration and implications of uncertain projections, Geosci. Model Dev., 16, 7171–7201, https://doi.org/10.5194/gmd-16-7171-2023, 2023.

Swiss phenology network: https://www.meteoswiss.admin.ch/weather/measurement-systems/land-based-stations/swiss-phenology-network.html, last access: 29 January 2025.

Pinheiro, J. C. and Bates, D. M.: Mixed-effects models in S and S-PLUS, Springer, New York, 528 S. pp., 2000.

R Core Team: R: A language and environment for statistical computing. R Foundation for Statistical Computing, 2022.

Shaw, H. G.: Centigrade-Fahrenheit temperature conversion, J. Chem. Educ., 8, 727, 1931.

Sitch, S., Prentice, I. C., Smith, B., Cramer, W., Kaplan, J. O., Lucht, W., Sykes, M. T., Thonicke, K., and Venevsky, S.: LPJ - A Coupled Model Of Vegetation Dynamics And The Terrestrial Carbon Cycle. https://www.researchgate.net/publication/37456884, 2000.

Wasserman, L.: All of Statistics. A Concise Course in Statistical Inference, 1st ed., Springer New York, NY, 2004.

Wohlfahrt, G. and Gu, L.: The many meanings of gross photosynthesis and their implication for photosynthesis research from leaf to globe, Plant Cell Environ., 38, 2500–2507, https://doi.org/10.1111/pce.12569, 2015.

Wood, S. N.: Fast stable restricted maximum likelihood and marginal likelihood estimation of semiparametric generalized linear models, J. R. Stat. Soc. Ser. B Stat. Methodol., 73, 3–36, https://doi.org/10.1111/j.1467-9868.2010.00749.x, 2011.

Wood, S. N.: Generalized additive models: An introduction with R, 2nd edition., Chapman and Hall/CRC, New York, 2017.

Woods, H. W.: Centigrade-fahrenheit temperature conversion, J. Chem. Educ., 8, 370, 1931.

Xiang, Y., Sun, D. Y., Fan, W., and Gong, X. G.: Generalized Simulated Annealing algorithm and its application to the Thomson model, Phys. Lett. A, 233, 216–220, https://doi.org/10.1016/s0375-9601(97)00474-x, 1997.

Xiang, Y., Gubian, S., and Martin, F.: Generalized Simulated Annealing, in: Computational Optimization in Engineering - Paradigms and Applications, 25–46, 2017.

Yates, F.: The analysis of multiple classifications with unequal numbers in the different classes, J. Am. Stat. Assoc., 29, 51–66, https://doi.org/10.2307/2278459, 1934.

Zani, D., Crowther, T. W., Mo, L., Renner, S. S., and Zohner, C. M.: Increased growing-season productivity drives earlier autumn leaf senescence in temperate trees, Science, 370, 1066–1071, https://doi.org/10.1126/science.abd8911, 2020.